Optically detected magnetic resonance in (Zn,Mn)Se/(Zn,Be)Se quantum wells

V. Yu. Ivanov,[1] M. Godlewski,[1,2] D. R. Yakovlev,[3,4] M. K. Kneip,[3] M. Bayer,[3] S. M. Ryabchenko,[5] and A. Waag[6]

[1]*Institute of Physics, Polish Academy of Sciences, 02-668 Warsaw, Poland*
[2]*Department of Mathematics and Natural Sciences College of Science, Cardinal Stefan Wyszynski University, 01-815 Warsaw, Poland*
[3]*Experimentelle Physik II, Technische Universität Dortmund, D-44221 Dortmund, Germany*
[4]*A. F. Ioffe Physico-Technical Institute, Russian Academy of Sciences, 194017 St. Petersburg, Russia*
[5]*Institute of Physics NAS of Ukraine, Kyiv 680028, Ukraine*
[6]*Institute of Semiconductor Technology, Braunschweig Technical University, 38106 Braunschweig, Germany*

The effects of microwave radiation with a frequency of 60 GHz on the magneto-optical properties of diluted magnetic semiconductors are studied on (Zn,Mn)Se/(Zn,Be)Se quantum wells. Resonant heating of the Mn^{2+} ions leads to an increase in the Mn-spin temperature as detected by the shift of emission line and increase in emission intensity. Nonresonant heating mediated by free carriers is also observed through variation in the polarization degree of emission. The mechanisms of optically detected magnetic resonance in diluted magnetic semiconductors are discussed.

PACS number(s): 71.35.Ji, 72.25.Rb, 75.50.Pp, 76.70.Hb

I. INTRODUCTION

Optical detection of microwave (MW)–induced effects in semiconductors is a well established experimental technique.[1,2] It has been widely used to study the energy and spin structure of excitons and impurity centers as well as their formation dynamics. The technique is especially suitable for nanostructures where the small amount of active material is not sufficient for application of electron-spin-resonance (ESR) methods.[3] Further, the spectral selectivity also allows investigation of different layers, e.g., quantum wells of different thicknesses, in the same structure. The microwave frequency range used in these investigations commonly covers 10–130 GHz and can be extended to higher frequencies. This range is mostly suited for resonant excitation of spin splitted electronic levels and therefore the technique is often called optically detected magnetic resonance (ODMR).

ODMR has been intensively applied for studying diluted magnetic semiconductors (DMSs). Using Faraday rotation for optical detection of the effect, Komarov *et al.*[4] discovered in 1977 the giant exchange interaction of free carriers with the localized spins of magnetic ions, promoting the new class of DMS materials. Later, ODMR was used for investigation of (Zn,Mn)Te,[5] (Cd,Mn)Te,[6–8] and (Zn,Mn)S (Ref. 9) bulk DMSs. Optical detection can be realized by Faraday or Kerr rotation, emission and reflectivity spectroscopies, and also Raman scattering. Very recently a new method has been implemented for DMS studies in the form of coherent Raman-detected electron-spin-resonance spectroscopy (CRESR).[10]

Microwave-induced effects on the optical properties of DMS are very pronounced as they address their giant signatures of Faraday and Kerr rotation or of Zeeman splitting of the band states of free carriers. They can be seen as shifts of transition energy, variations in signal intensity, or changes in polarization degree in optical spectra. The characteristics of these effects are controlled by energy and spin transfer between three interacting systems in the DMS: the Mn-spin system, the phonon system (lattice), and the free carriers.[11–15] Microwaves can heat the Mn-spin system, e.g., resonantly under the condition of electron-spin resonance when the MW photon is resonant with the spin splitting of a Mn^{2+} ion. The MW energy can be absorbed also by free carriers, e.g., electrons, under conditions of either spin resonance or cyclotron resonance. The latter can be rather broad due to very short momentum relaxation time of electrons in II-VI semiconductors and very often it can be treated as nonresonant heating of the electrons by increasing their kinetic energy.

Hot carriers can efficiently transfer their energy further to the Mn system.[13,14] Cooling of the Mn-spin system is provided by spin-lattice relaxation (SLR), which transfers the energy to the phonon bath. In II-VI DMSs the SLR dynamics of the Mn-spin system covers a wide temporal range from milliseconds down to nanoseconds, depending strongly on the Mn content.[16,17] A technique to study the SLR dynamics by pulsed MW excitation was demonstrated recently.[18] Among the advantages of using MWs to study the spin dynamics of magnetic ions and carriers is the possibility of addressing exclusively the Mn-spin system under ESR conditions. This simplifies considerably the interpretation of experimental data, compared to the case of laser heating of DMS.[14,16]

Only recently the ODMR technique was applied to DMS nanostructures: (Cd,Mn)Te/(Cd,Mg)Te (Refs. 19 and 20) and (Zn,Mn)Se/(Zn,Be)Se (Ref. 18) quantum wells (QWs). Resonant heating of the Mn system was detected by monitoring the spectral shift of emission lines and the redistribution of intensity between the neutral and negatively charged exciton (trion, which is a three-body complex that involves an exciton and an extra electron) emission lines.

The goal of this paper is to provide a detailed experimental study of microwave-induced effects in DMS quantum wells based on (Zn,Mn)Se/(Zn,Be)Se heterostructures. The mechanisms of the induced effects and their appearances in magneto-optical spectra are discussed.

II. EXPERIMENT

The ODMR spectrometer used for this study consists of a 60 GHz all-solid-state MW oscillator (photon energy, 0.248 meV) with an output power of up to 300 mW. The output power of the oscillator can be varied up to 40 dB attenuation level. The oscillator can operate either in continuous-wave (cw) mode or in a periodically pulsed mode with an on-off transition time of about 3 ns at more than 60 dB dumping level. The sample is mounted in a cylindrical H_{011} microwave cavity (with low Q factor of about 600). The cavity has two orthogonal pairs of apertures with a conic cross section for illumination of the samples and collecting the sample emission. The sample located in the cavity is excited by a laser along its growth axis, which is oriented parallel to an external magnetic field generated by a split-coil superconducting magnet with a maximum field of 7 T. The cavity is placed in the variable-temperature insert of the magnetic cryostat. A schema of the setup is given in Ref. 18.

All experiments reported in this paper are performed with the samples immersed in pumped liquid helium at a temperature $T = 1.6$ K. The output power of the MW oscillator is 260 mW. The photoluminescence (PL) was excited by an (In-,Ga)N semiconductor laser with a wavelength of 404 nm (photon energy, 3.07 eV). The density of photoexcitation is kept at a low level of 0.02 W/cm^2 in order to minimize additional heating of the Mn-spin system. In the continuous-wave regime the luminescence spectra are detected by a charge-coupled-device (CCD) camera synchronously with switching the MW on and off (typical switching period is about 100 ms). Magnetic-field dependencies of the MW-induced effects are obtained by scanning the magnetic field.

For time-resolved experiments a periodic train of MW pulses with a duration of 2 ms at a frequency of 250 Hz is used. The kinetics of the changes induced in the optical spectra was measured at a fixed magnetic field right after the MW pulse. The fall of the MW pulses is synchronized with the start of a time-correlated single-photon counting system by a high-precision digital delay generator. The PL kinetics is measured sequentially at different spectral positions using a single-photon detector (photomultiplier) which allows us to analyze the temporal evolution of the PL spectra (peak amplitude and spectral shape).

Results for two samples are reported in this paper. Both are $Zn_{1-x}Mn_xSe/Zn_{1-y}Be_ySe$ multiple quantum well (MQW) structures grown by molecular-beam epitaxy on (100)-oriented GaAs substrates. The substrates were overgrown by a buffer consisting of 1-nm-thick BeTe, 2-nm-thick ZnSe, and 400-nm-thick $Zn_{0.97}Be_{0.03}Se$ layers, to improve the surface quality and the lattice matching with the barrier material. On top of that the MQW was grown. The first sample (cb1541) contains five periods of 10-nm-thick $Zn_{0.988}Mn_{0.012}Se$ wells separated by 20-nm-thick $Zn_{0.94}Be_{0.06}Se$ barriers. The second sample (cb1433) contains ten periods of 20-nm-thick $Zn_{0.94}Mn_{0.06}Se$ wells separated by 10-nm-thick $Zn_{0.95}Be_{0.05}Se$ barriers. The samples were nominally undoped, so that the background electron density in the wells does not exceed 10^{10} cm^{-2}. Details on the magneto-optical properties of these samples can be found in Refs. 13 and 16. Differences in well width of the samples are not
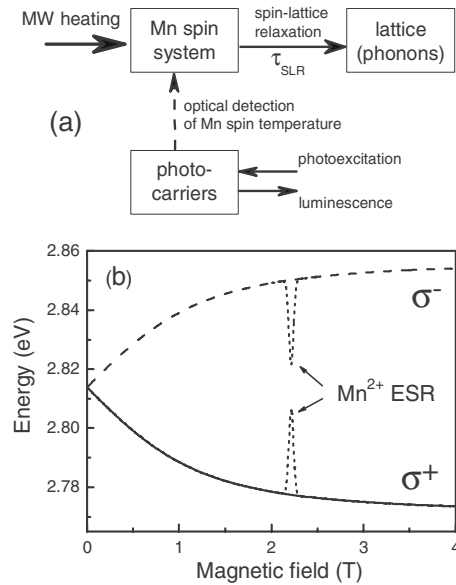
FIG. 1. (a) Scheme of spin and energy reservoirs in DMS. Pathways for energy and spin transfers between these reservoirs are shown by arrows. Microwaves provide a direct heating of the Mn-spin system; photocarriers are used for detection of the Mn-spin temperature. (b) Giant Zeeman splitting of exciton states calculated for $Zn_{0.988}Mn_{0.012}Se$ at $T = 1.6$ K (parameters are given in text). The short-dashed line shows resonant decrease in the Zeeman splitting under condition of electron-spin resonance of the Mn^{2+} ions applying 60 GHz MW radiation.

important for our study, but the different Mn contents of 0.012 and 0.06 are of key importance. Note that the MQWs have a type-I band alignment; i.e., both electrons and holes are confined in the DMS $Zn_{1-x}Mn_xSe$ quantum well layers. Moreover the width of the wells and height of the barriers are sufficiently large to prevent strong leakage of the carrier wave functions into the nonmagnetic barriers.

III. RESULTS AND DISCUSSION

The spin dynamics of carriers and magnetic ions in DMS is controlled by the interaction of three systems: carriers, Mn ions, and lattice. Energy and spin transfers between them control the DMS magnetization. These systems are shown schematically in Fig. 1(a). The energy- and spin-transfer pathways important for ODMR are indicated by the arrows. Here MW energy is absorbed by the Mn-spin system, which renders its energy to the lattice via the spin-lattice interaction on a characteristic time scale τ_{SLR}. The photocarriers are used only for the optical detection of the Mn-spin temperature T_{Mn}, e.g., through the high-energy shift of the PL line. The energy flux from the carriers to the Mn system is vanishingly small as very low laser excitation densities are used, and it therefore does not change T_{Mn}.

II-VI DMSs with Mn ions offer a convenient method to evaluate the temperature of the Mn-spin system, which has been widely used in studies of the magnetization dynamics.[12,17] The internal Mn-spin thermometer is based on the high sensitivity of the giant Zeeman splitting of the ex-

citons to the polarization of the Mn spins in an external magnetic field.

The giant Zeeman splitting is proportional to the magnetization and therefore to the average spin of the Mn ions. For heavy-hole excitons in bulk DMS the splitting is described by

$$\Delta E_z = (N_0\alpha - N_0\beta)x\langle S_z\rangle. \tag{1}$$

Here $N_0\alpha = 0.26$ eV and $N_0\beta = -1.31$ eV are the exchange constants in $Zn_{1-x}Mn_xSe$ for the conduction and valence bands, respectively.[21] x is the Mn mole fraction. $\langle S_z\rangle$ is the thermal mean value of the Mn-spin component along the magnetic field $B=B_z$ at a Mn-spin temperature T_{Mn}. It is expressed by the modified Brillouin function $B_{5/2}$:

$$\langle S_z\rangle = -S_{eff}(x)B_{5/2}\left[\frac{5g_{Mn}\mu_B B}{2k_b[T_{Mn} + T_0(x)]}\right]. \tag{2}$$

Here $g_{Mn} = 2$ is the g factor of the Mn^{2+} ions. S_{eff} is the effective spin and T_0 is the effective temperature. These parameters permit a phenomenological description of the antiferromagnetic Mn-Mn exchange interaction. Their values for $Zn_{1-x}Mn_xSe$ can be found in Ref. 13.

An example of the giant Zeeman splitting of excitons in $Zn_{0.988}Mn_{0.012}Se$, i.e., for the Mn content of the first sample, is given in Fig. 1(b). It has been calculated using Eqs. (1) and (2) with $S_{eff} = 2.21$, $T_0 = 0.5$ K,[13] and $T_{Mn} = 1.6$ K. Only the lower component of the two lines, which is σ^+ circularly polarized, can be seen in photoluminescence, and both components can be detected in reflectivity or transmission spectra.

An increase in the Mn-spin temperature would cause a decrease in the giant Zeeman splitting [see Eq. (2)]. In Fig. 1(b) this is shown schematically for the resonant heating of the Mn^{2+} ions by 60 GHz MW radiation up to $T_{Mn} \approx 20$ K. The MW-induced resonant decrease in the Zeeman splitting is expected to occur at a magnetic field of $B_R = 2.14$ T, corresponding to a Mn^{2+} ion g factor $g_{Mn} = 2.0069 \pm 0.0005$ in (Zn,Mn)Se.[22] We will show below that this behavior is indeed observed in (Zn,Mn)Se-based QWs.

The evolution of the luminescence spectra of the $Zn_{0.988}Mn_{0.012}Se/Zn_{0.94}Be_{0.06}Se$ MQW in an external magnetic field is displayed in Fig. 2. In panel (a) it is shown without MW application. At zero magnetic field the spectrum has two lines. The higher-energy one with a maximum at 2.813 eV is related to neutral excitons (X) and the one with the maximum at 2.808 eV is due to negatively charged excitons (trions, T); for details see Ref. 13. With increasing magnetic field both lines shift to lower energies. The trion line loses intensity and becomes invisible for fields above 0.32 T. This well-known effect is due to ionization of the negatively charged exciton with two electrons in the singlet state when the giant Zeeman splitting in the conduction band exceeds the trion binding energy.[23,24] The same mechanism is responsible for suppression of the donor-bound exciton emission in bulk DMS.[25] One sees also that the integral intensity of the excitonic emission increases strongly with increasing magnetic field. This behavior is well known for (Zn,Mn)Se-based
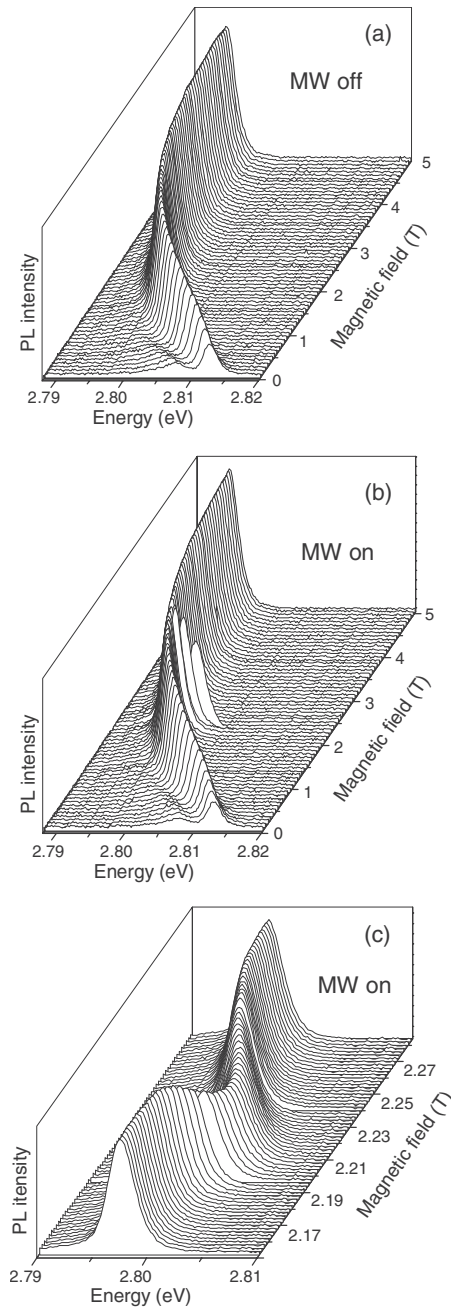
FIG. 2. Evolution of photoluminescence spectra in a $Zn_{0.988}Mn_{0.012}Se/Zn_{0.94}Be_{0.06}Se$ MQW with increasing magnetic field: (a) without MW, (b) with MW at full power, and (c) in the vicinity of the Mn^{2+} electron-spin resonance. $T = 1.6$ K.

DMS and explained by a competition of the excitonic emission with nonradiative channels and internal Mn^{2+} transitions.[26–28]

When the MW is switched on, the field evolution of PL spectra is not modified significantly except for the ESR region around 2.1 T. The whole field range is shown in panel (b) and the resonance part is detailed in panel (c) of Fig. 2.

PL spectra with and without MW are compared in Fig. 3. At the ESR magnetic field of 2.138 T, strong changes in both energy shift and peak intensity occur. Considerably weaker MW-induced changes can be also seen at nonresonant con-
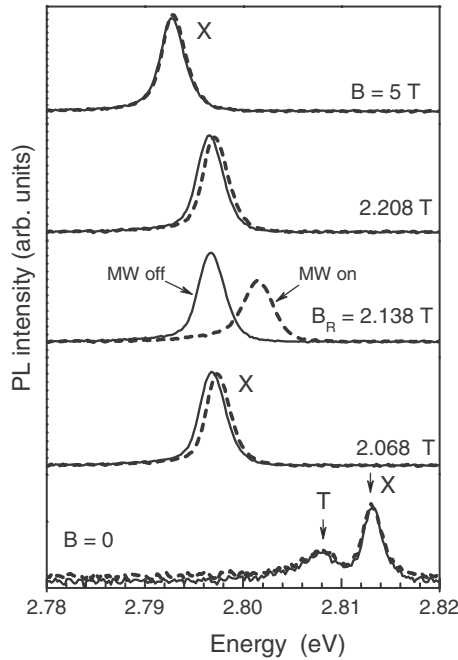
FIG. 3. Photoluminescence spectra of a $Zn_{0.988}Mn_{0.012}Se/Zn_{0.94}Be_{0.06}Se$ MQW measured at $T=1.6$ K with a photoexcitation density of 0.02 W/cm^2 at different magnetic fields. Exciton (X) and trion (T) lines are seen at $B=0$ T. With increasing field the trion line is ionized and the exciton line dominates the spectrum. The MW power is 260 mW. A strong shift of the exciton line at about 2.14 T when the ESR condition is met is clearly seen.

ditions for $B=2.068$ and 2.208 T, and they are even detectable at high magnetic fields of $B=5$ T.

These changes can be explained by indirect heating of the Mn-spin system via free carriers. The MW is first absorbed by the resident electrons, increasing their kinetic energy. Then the energy is transferred to the Mn-spin system via exchange scattering of the electrons with the localized magnetic moments of the Mn ions. Even though nominally undoped, (Zn,Mn)Se and ZnSe-based heterostructures grown by molecular-beam epitaxy show a residual *n*-type doping in the quantum well and barrier layers. The donor electrons captured by the QWs form a diluted two-dimensional electron gas (2DEG), whose density typically does not exceed 10^{10} cm^{-2}.[13,29] The presence of the 2DEG is confirmed by observation of negatively charged excitons in the PL spectra. At such low densities the resident electrons are predominantly localized in the well width fluctuations. The low mobility of these electrons does not allow observation of a pronounced cyclotron resonance under MW radiation. Instead their contribution shows up as a broad tail in the MW-induced changes as function of magnetic field (see Figs. 4–6).

Let us first discuss the energy shift of the PL line. This shift is caused by the reduction in the giant Zeeman splitting of the excitons, which in turn reflects the heating of the Mn-spin system. The energy positions of the PL lines measured with and without MW are plotted in Fig. 4(a) as a function of magnetic field. The changes are very pronounced for resonant conditions at $B_R=2.138$ T ($g_{Mn}=2.0068$). The nonreso-
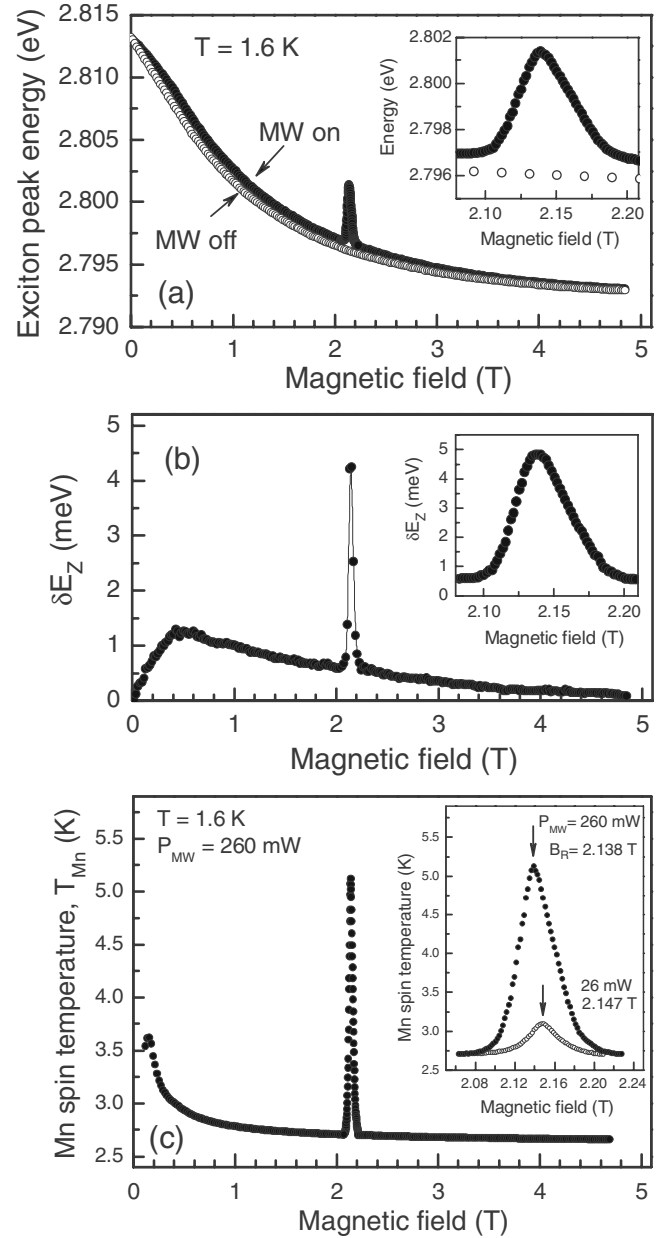
FIG. 4. Microwave effect on the energy shift of the PL line in a $Zn_{0.988}Mn_{0.012}Se/Zn_{0.94}Be_{0.06}Se$ MQW. (a) Giant Zeeman shift of the σ^+-polarized emission. The photoexcitation density is 0.02 W/cm^2. The MW power is 260 mW. The inset shows the field range around the ESR resonant field. (b) Microwave-induced energy shift versus magnetic field. The inset shows the field range around the ESR resonant field. (c) Magnetic-field dependence of the Mn-spin temperature evaluated from the energy shift of emission line in panel (b). Full MW power (0 dB attenuation) is applied. In the inset the increase in the Mn-spin temperature is shown in the vicinity of the ESR for two MW powers.

nant changes are seen over the whole range of magnetic fields, as seen more clearly from the MW-induced shift $\delta E_z(B)$ plotted in panel (b). The nonresonant shift shows a nonmonotonic behavior: It increases up to 0.5 T and then decreases with increasing magnetic field. This is the result of the combined contributions of the magnetic-field dependencies of: (i) the giant Zeeman splitting described by the modi-
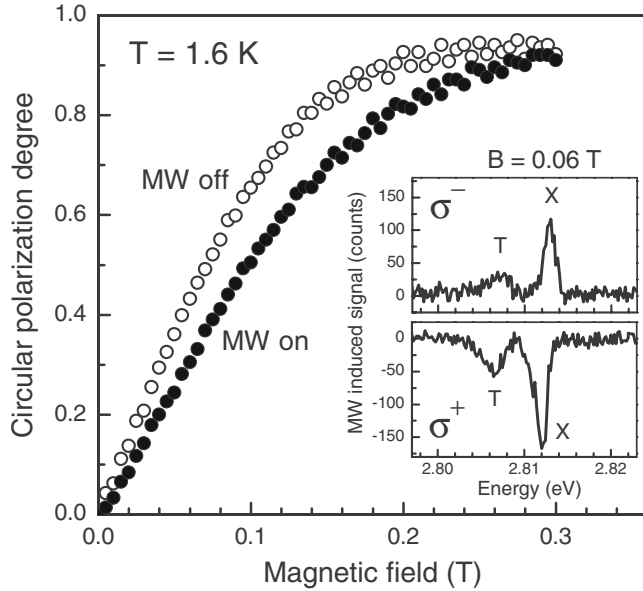
FIG. 5. Circular polarization degree of PL, P_c, measured with and without MW. In the inset the MW effects for different circular polarizations are shown. The MW-induced signal is the difference between PL intensities measured with and without MW.

fied Brillouin function, (ii) the carrier heating efficiency by the MW, and (iii) the spin-lattice relaxation time of Mn ions.[30]

For our study it is more convenient to analyze the magnetic-field dependence of the Mn-spin temperature, which can be evaluated from the giant Zeeman splitting of the heavy-hole excitons in (Zn,Mn)Se/(Zn,Be)Se quantum wells. In the case of a DMS quantum well, the equation for the exciton giant Zeeman splitting differs from Eq. (1) describing bulk DMS for two reasons. First, the parameters α and β depend in a QW on the z coordinate through the dis-
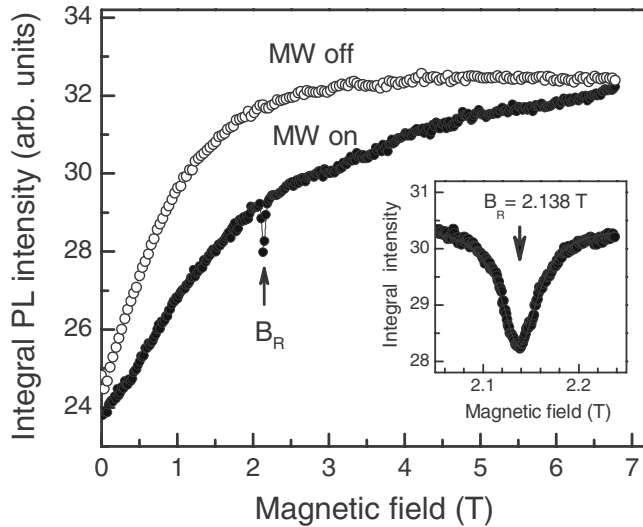
FIG. 6. Integral PL intensity of exciton and trion lines as a function of magnetic field in a $Zn_{0.988}Mn_{0.012}Se/Zn_{0.94}Be_{0.06}Se$ MQW. Dependences for the "on" and "off" MW conditions are shown. The inset is a closeup of the part in the vicinity of the ESR. T=1.6 K.
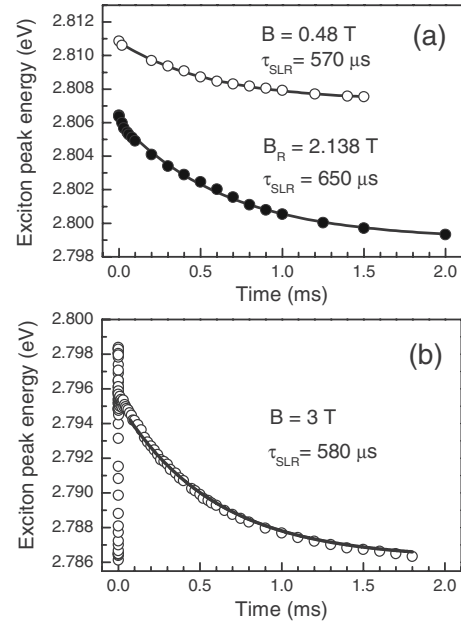
FIG. 7. Kinetics of the exciton line shift after switching off the MW pulse for a $Zn_{0.988}Mn_{0.012}Se/Zn_{0.94}Be_{0.06}Se$ MQW. Experimental data for magnetic fields of 0.48 and 2.138 T are given by the symbols. The lines are single exponential fits with time constants denoted in the figure. (a): measured under pulsed MW; (b): measured under laser photoexcitation with a 7 ns pulsed laser (355 nm). T=1.6 K.

tribution of the confined wave functions for electrons and holes. Second, a part of the carrier wave function may leak from the DMS quantum well layer into the nonmagnetic barriers. However, the splitting of the heavy-hole exciton in quantum wells subject to a magnetic field applied along the structure growth axis (Faraday geometry) can be calculated by

$$\Delta E_z^{QW} = (\delta_e N_0 \alpha - \delta_h N_0 \beta) x \langle S_z \rangle, \qquad (3)$$

using the bulk values of $N_0\alpha$ and $N_0\beta$. Here the parameters δ_e and δ_h characterize the leakage of the electron and hole wave functions into the barriers. Their values ranges from 1 to 0 for wave functions fully confined in the well and in the barrier layers, respectively.[16] In our case of wide QW $\delta_e \approx \delta_h \approx 1$.

The dependence $T_{Mn}(B)$ in Fig. 4(c) has been obtained from the experimental data in Fig. 4(b) by converting the energy shift into T_{Mn} using Eqs. (2) and (3). A Mn-spin temperature of 5.2 K is achieved under ESR conditions.

We recall that the sample is immersed in pumped liquid helium at a bath temperature of 1.6 K and the lattice heating does not exceed 1 K. Such an efficient resonant heating of the Mn-spin system means that the spin system is weakly coupled to the lattice [see the scheme in Fig. 1(a)]. Spin-lattice relaxation in $Zn_{0.988}Mn_{0.012}Se$ occurs on a millisecond time scale as shown in Fig. 7 for the studied sample. Therefore, the MW energy absorbed by the Mn^{2+} ions cannot be forwarded fast enough to the lattice and is stored in the spin system, increasing its temperature. The Mn heating is also detectable for nonresonant conditions. It gains about 1 K

overheating at low magnetic fields but nearly vanishes at 5 T. We suggest that for $B < 1$ T the field dependence of heating is mainly controlled by the carrier heating efficiency, i.e., by the broadened cyclotron resonance. For $B > 1$ T it is due to the shortening of the SLR time of the Mn ions (see Fig. 2 of Ref. 30).

In very weak magnetic fields below 0.1–0.3 T, the spectral resolution of the changes of the giant Zeeman splitting by MW is limited by the inhomogeneous broadening of the exciton lines. It becomes especially important for increasing Mn content and in narrow quantum wells (see, e.g., Ref. 31). In this case the changes in magnetization and T_{Mn} can be traced by measuring the circular polarization degree (P_c) of the exciton emission.[5,13,29]

We perform such experiments for the $Zn_{0.988}Mn_{0.012}Se/Zn_{0.94}Be_{0.06}Se$ MQW. One sees in Fig. 5 that $P_c = (I^+ - I^-)/(I^+ + I^-)$, where I^+ and I^- are the PL intensities of σ^+- and σ^--polarized emission, decreases under MW application, evidencing heating of the Mn system. The spectral changes in the PL emission are given in the inset for $B = 0.06$ T. The MW-induced signal in this case is just the difference between PL intensities with and without MW. One can see that the effect of MW is opposite for σ^+ and σ^- polarization. This behavior is expected as the heating of the Mn system reduces the giant Zeeman splitting of the exciton, which in turn reduces the thermal occupation of the lowest Zeeman level, providing σ^+-polarized emission, and vice versa increases the occupation of the upper Zeeman level, leading to σ^--polarized emission.

We turn now to the effect of the magnetic field on the integral exciton emission. Its increase with magnetic field has been noted already in connection with Fig. 2. The integral PL intensity, which includes the exciton and trion lines in both polarizations, is plotted in Fig. 6 as a function of magnetic field. It increases steadily by about 30% at $B = 3$ T and then saturates at higher fields. This dependence is very similar to the behavior of the exciton giant Zeeman splitting shown in Fig. 1(b). Therefore one can conclude that the change in the integral intensity is proportional to the magnetization, i.e., proportional to the polarization of the Mn^{2+} spins. The clarification of the underlying mechanism is beyond the scope of this paper. In literature no final agreement about the origin has been reached. Among the suggested origins are spin dependent Auger recombination of excitons interacting with Mn^{2+} ions[26] and spin dependent transfer of excitation from excitons to Mn^{2+} internal transitions.[28]

Under MW radiation the integral intensity decreases, especially at the resonance magnetic field B_R, in line with the conclusion that the PL intensity is controlled by the magnetization. Both resonant and nonresonant heating of the Mn-spin system can be seen by this method.

The magnetization dynamics can be also studied by the ODMR technique. For that purpose one has to perform experiments with proper time resolution to trace, e.g., the cooling of the Mn-spin system after being heated by pulsed MW. This allows one to measure the spin-lattice relaxation rate. The relaxation dynamics of the energy shift of the exciton line after the MW pulse is shown in Fig. 7(a). Kinetic measurements at resonant and nonresonant magnetic fields give
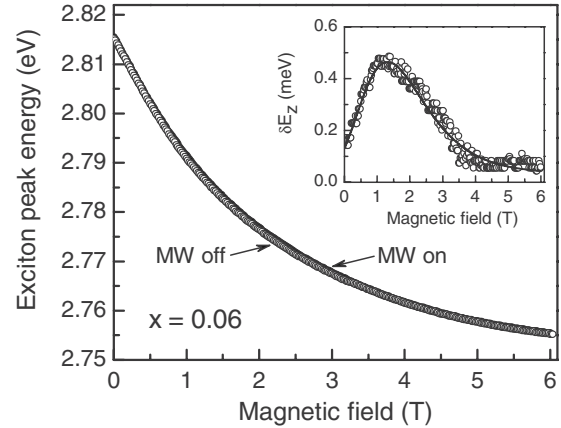
FIG. 8. Dependence of the exciton PL line peak position in a $Zn_{0.94}Mn_{0.06}Se/Zn_{0.95}Be_{0.05}Se$ MQW on the magnetic field measured with (closed symbols) and without (open symbols) MW. The photoexcitation density is 0.02 W/cm², at full MW power (attenuation, 0 dB). $T = 1.6$ K. The MW-induced energy shift is given in the inset.

very similar SLR times of 650 and 570 μs, respectively. This evidences that the relaxation dynamics is not very sensitive to the value of T_{Mn} but is rather controlled by the bath temperature and the Mn content.[17]

We have examined the magnetization dynamics in the $Zn_{0.988}Mn_{0.012}Se/Zn_{0.94}Be_{0.06}Se$ MQW by a time-resolved technique based on laser heating of the Mn-spin system (details can be found in Refs. 14 and 16). Laser pulses with 7 ns duration at a photon energy of 3.49 eV are used to bring the Mn-spin system out of equilibrium with the lattice. The time evolution of the peak energy is displayed in Fig. 7(b). The relaxation rate of 580 μs measured at $B = 3$ T is in good agreement with the ODMR data from panel (a), confirming the validity of the both techniques.

In the $Zn_{0.94}Mn_{0.06}Se/Zn_{0.95}Be_{0.05}Se$ MQW with higher Mn content ($x = 0.06$), the effects of the MW are considerably weaker compared to the sample with $x = 0.012$. One can see in Fig. 8 that the energy shift of the exciton line in external magnetic field is hardly sensitive to MW radiation. Its maximal shift does not exceed 0.5 meV, which is observed at $B = 1.2$ T, corresponding to elevation of T_{Mn} by about 0.1 K only. The reason is the fast spin-lattice relaxation, whose characteristic time for $x = 0.06$ is about 1 μs,[16] i.e., nearly 3 orders of magnitude shorter than for $x = 0.012$. The efficient cooling prevents a strong MW heating of the Mn-spin system. We do not observe any resonant signal in the vicinity of the expected $B_R = 2.138$ T. One of the reasons for that may be the broadening of the ESR due to Mn-Mn interactions, which is drastically enhanced for higher Mn contents.

Let us return now to the inset of Fig. 4(c) and discuss the effect of the MW power on the resonance field B_R in the $Zn_{0.988}Mn_{0.012}Se/Zn_{0.94}Be_{0.06}Se$ MQW. Attenuation of the MW power by 10 dB (down to 26 mW) causes a shift of B_R from 2.138 to 2.146 T. In addition the Mn-spin temperature achieved for attenuated power was 3.2 K only, compared to the 5.2 K for full MW power. The shift can be explained by the contribution of the surface demagnetization to the resonance field:[32]

$$B_R = \frac{\hbar\omega_{MW}}{g_{Mn}\mu_B} + 4\pi M(T_{Mn}). \tag{4}$$

Estimations for $x=0.012$ and $B=2$ T give a shift of 16 mT for $T_{Mn}=3.2$ K and 9 mT for $T_{Mn}=5.2$ K. This is in good agreement with the 8 mT difference shown in the inset of Fig. 4(c). It is worthwhile to note that for (Cd,Mn)Te samples with a very low Mn concentration of $x=0.005$, the fine-structure splitting of the Mn^{2+} ion in magnetic field was observed in the ODMR spectrum.[33]

To summarize, there is a variety of microwave-induced effects which allow optical detection of the Mn-spin temperature in II-VI DMSs. Most of them are not specific for low-dimensional systems but can be applied also to bulk, quantum well, and quantum dot systems containing DMSs. The common feature of all these effects is their strong dependence on the magnetization. At least four of them can be suggested on the base of the present work and the preceding reports:

(1) The spectral shift of the exciton resonance, which is the most direct consequence of the reduction in the giant Zeeman splitting.[5–7] It gives the clearest signature except of very weak magnetic fields, where polarization mechanism 2 is stronger.

(2) The variation in the circular polarization degree of the exciton luminescence, namely, its decrease under MW heating.[5,13]

(3) The variation in the exciton integral intensity.

(4) The changes in the shape of exciton line in emission, absorption, or transmission. These changes can be variation in the broadening of a single line or intensity redistribution between different lines in emission spectra. An example of the latter is the interplay between the exciton and negatively charged exciton lines in quantum wells or between the bound and free exciton lines in bulk DMS.[23,25,33]

Very often combinations of these effects contribute to the ODMR spectra. Thus it might be challenging to distinguish their separate contributions.

IV. CONCLUSIONS

Using (Zn,Mn)Se-based DMS quantum well structures as an example, we have shown that the ODMR technique is a very efficient tool to study the magnetization of the Mn-spin system and its dynamics. In addition to the energy shift of the exciton line caused by suppression of the giant Zeeman splitting, the MW interferes with the circular polarization degree and the exciton emission intensity. A comparative study of the spin-lattice relaxation dynamics by using MW heating on one hand and by laser excitation on the other hand gives similar values for the relaxation times, confirming the validity of both techniques. The MW heating is efficient in the sample with low Mn content $x=0.012$, where the Mn-spin temperature was elevated by 2.5 K, but is weak for higher Mn content $x=0.06$, where the maximal heating does not exceed 0.1 K. Very different spin-lattice relaxation times are responsible for this difference.

[1] B. C. Cavenett, Adv. Phys. **30**, 475 (1981).

[2] M. Godlewski, W. M. Chen, and B. Monemar, CRC Crit. Rev. Solid State Mater. Sci. **19**, 241 (1994).

[3] P. G. Baranov and N. G. Romanov, Appl. Magn. Reson. **21**, 165 (2001).

[4] A. V. Komarov, S. M. Ryabchenko, O. V. Terletskii, I. I. Zheru, and R. D. Ivanchuk, Zh. Eksp. Teor. Fiz. **73**, 608 (1977) [Sov. Phys. JETP **46**, 318 (1977)].

[5] A. V. Malyavkin, Phys. Status Solidi B **115**, 353 (1983).

[6] A. V. Malyavkin and A. A. Dremin, JETP Lett. **42**, 114 (1985) [Pis'ma Zh. Eksp. Teor. Fiz. **42**, 95 (1985)].

[7] S. J. C. H. M. van Gisbergen, M. Godlewski, R. R. Galazka, T. Gregorkiewicz, C. A. J. Ammerlaan, and N. T. Khoi, Phys. Rev. B **48**, 11767 (1993).

[8] S. Zeng, L. C. Smith, J. J. Davies, D. Wolverson, S. J. Bingham, and G. N. Aliev, Phys. Status Solidi B **243**, 887 (2006).

[9] V. Yu. Ivanov, M. Godlewski, S. Yatsunenko, A. Khachapuridze, M. S. Li, and Z. Golacki, Acta Phys. Pol. A **100**, 351 (2001).

[10] L. C. Smith, D. Wolverson, S. J. Bingham, and J. J. Davies, Phys. Status Solidi B **243**, 892 (2006).

[11] M. Godlewski, R. R. Galazka, I. Tsimperidis, T. Gregorkiewicz, and C. A. J. Ammerlaan, Acta Phys. Pol. A **87**, 177 (1995).

[12] D. R. Yakovlev, Phys. Status Solidi A **204**, 179 (2007).

[13] D. Keller, D. R. Yakovlev, B. Konig, W. Ossau, Th. Gruber, A. Waag, L. W. Molenkamp, and A. V. Scherbakov, Phys. Rev. B **65**, 035313 (2001).

[14] M. K. Kneip, D. R. Yakovlev, M. Bayer, A. A. Maksimov, I. I. Tartakovskii, D. Keller, W. Ossau, L. W. Molenkamp, and A. Waag, Phys. Rev. B **73**, 035306 (2006).

[15] M. Godlewski, Opt. Appl. **36**, 271 (2006).

[16] M. K. Kneip, D. R. Yakovlev, M. Bayer, A. A. Maksimov, I. I. Tartakovskii, D. Keller, W. Ossau, L. W. Molenkamp, and A. Waag, Phys. Rev. B **73**, 045305 (2006).

[17] A. V. Akimov, A. V. Scherbakov, and D. R. Yakovlev, in *Handbook of Semiconductor Nanostructures and Nanodevices*, edited by A. A. Balandin and K. L. Wang (American Scientific, Los Angeles, 2006), Chap. 2, p. 45.

[18] V. Yu. Ivanov, M. Godlewski, D. R. Yakovlev, S. M. Ryabchenko, G. Karczewski, and A. Waag, Phys. Status Solidi A **204**, 174 (2007).

[19] M. Godlewski, V. Yu. Ivanov, A. Khachapuridze, and S. Yat-sunenko, Phys. Status Solidi B **229**, 533 (2002).

[20] M. L. Sadowski, M. Byszewski, M. Potemski, A. Sachrajda, and G. Karczewski, Appl. Phys. Lett. **82**, 3719 (2003).

[21] A. Twardowski, M. von Ortenberg, M. Demianiuk, and R. Pauthenet, Solid State Commun. **51**, 849 (1984).

[22] B. C. Cavenett, Proc. Phys. Soc. London **84**, 1 (1964).

[23] V. D. Kulakovskii, M. G. Tyazhlov, S. I. Gubarev, D. R. Yakovlev, A. Waag, and G. Landwehr, Nuovo Cimento D **17**, 1549 (1995).

[24] S. I. Gubarev, V. D. Kulakovskii, M. G. Tyazhlov, D. R. Yakovlev, A. Waag, and G. Landwehr, Ann. Phys. (Paris) **20**, C2 (1995).

[25] D. Heiman, P. Becla, R. Kershaw, D. Ridgley, K. Dwight, A. Wold, and R. R. Galazka, Phys. Rev. B **34**, 3961 (1986).

[26] M. Nawrocki, Yu. G. Rubo, J. P. Lascaray, and D. Coquillat, Phys. Rev. B **52**, R2241 (1995).

[27] B. Konig, U. Zehnder, D. R. Yakovlev, W. Ossau, T. Gerhard, M. Keim, A. Waag, and G. Landwehr, Phys. Rev. B **60**, 2653 (1999).

[28] H. Falk, J. Hubner, P. J. Klar, and W. Heimbrodt, Phys. Rev. B **68**, 165203 (2003).

[29] G. V. Astakhov, D. R. Yakovlev, V. P. Kochereshko, W. Ossau, W. Faschinger, J. Puls, F. Henneberger, S. A. Crooker, Q. McCulloch, D. Wolverson, N. A. Gippius, and A. Waag, Phys. Rev. B **65**, 165335 (2002).

[30] A. V. Scherbakov, D. R. Yakovlev, A. V. Akimov, I. A. Merkulov, B. Konig, W. Ossau, L. W. Molenkamp, T. Wojtowicz, G. Karczewski, G. Cywinski, and J. Kossut, Phys. Rev. B **64**, 155205 (2001).

[31] D. R. Yakovlev, U. Zehnder, W. Ossau, A. Waag, G. Landwehr, T. Wojtowicz, G. Karczewski, and J. Kossut, J. Magn. Magn. Mater. **191**, 25 (1999).

[32] Ch. Kittel, *Introduction to Solid State Physics*, 8th ed. (Wiley, New York, 2005), Chap. 13.

[33] M. Byszewski, D. Plantier, M. L. Sadowski, M. Potemski, A. Sachrajda, Z. Wilamowski, and G. Karczewski, Physica E (Amsterdam) **22**, 652 (2004).